Crystal Structural, Magnetic, and Transport Properties of Layered Cobalt Oxyfluorides, Sr2CoO3+xF1−x (0 <= x <= 0.15)

ARTICLE *in* INORGANIC CHEMISTRY · APRIL 2012

Impact Factor: 4.76 · DOI: 10.1021/ic300116h · Source: PubMed

Inorganic Chemistry

Article

pubs.acs.org/IC

Crystal Structural, Magnetic, and Transport Properties of Layered Cobalt Oxyfluorides, $Sr_2CoO_{3+x}F_{1-x}$ ($0 \leq x \leq 0.15$)

Yoshihiro Tsujimoto,*[,†] Clastin I. Sathish,[‡,§] Kun-Pyo Hong,[∥] Kengo Oka,[⊥] Masaki Azuma,[⊥] Yanfeng Guo,[§,⊗] Yoshitaka Matsushita,[○] Kazunari Yamaura,[‡,§,⊗] and Eiji Takayama-Muromachi[‡,§,⊗]

[†]International Center for Young Scientists (ICYS) and International Center for Materials Nanoarchitechtonics (WPI-MANA), National Institute for Materials Science (NIMS), Namiki 1-1, Tsukuba, Ibaraki 305-0044, Japan

[‡]Department of Chemistry, Graduate School of Science, Hokkaido University, Sapporo, Hokkaido 060-0810, Japan

[§]Superconducting Properties Unit, NIMS, Namiki 1-1, Tsukuba, Ibaraki 305-0044, Japan

[∥]Neutron Science Division, Department of Basic Science and Technology, Korea Atomic Energy Research Institute (KAERI), 1045, Daedeok-daero, Yuseon-gu, Daejeon, 305-353, Korea

[⊥]Materials and Structures Laboratory, Tokyo Institute of Technology, 4259 Nagatsuta, Midori-ku, Yokohama 226-8503, Japan

[⊗]JST, Transformative Research-Project on Iron Pnictides (TRIP), Namiki 1-1, Tsukuba, Ibaraki 305-0044, Japan

[○]NIMS Beamline Station at SPring-8, NIMS, 1-1-1 Kouto, Sayo-cho, Hyogo 679-5148, Japan

Supporting Information

ABSTRACT: The crystal structure of the layered cobalt oxyfluoride Sr_2CoO_3F synthesized under high-pressure and high-temperature conditions has been determined from neutron powder diffraction and synchrotron powder diffraction data collected at temperatures ranging from 320 to 3 K. This material adopts the tetragonal space group $I4/mmm$ over the measured temperature range and the crystal structure is analogous to $n = 1$ Ruddlesden−Popper type layered perovskite. In contrast to related oxyhalide compounds, the present material exhibits the unique coordination environment around the Co metal center: coexistence of square pyramidal coordination around Co and anion disorder between O and F at the apical sites. Magnetic susceptibility and electrical resistivity measurements reveal that Sr_2CoO_3F is an antiferromagnetic insulator with the Néel temperature $T_N = 323(2)$ K. The magnetic structure that has been determined by neutron diffraction adopts a G-type antiferromagnetic order with the propagation vector $k = (1/2\ 1/2\ 0)$ with an ordered cobalt moment $\mu = 3.18(5)\ \mu_B$ at 3 K, consistent with the high spin electron configuration for the Co^{3+} ions. The antiferromagnetic and electrically insulating states remain robust even against 15%-O substation for F at the apical sites. However, applying pressure exhibits the onset of the metallic state, probably coming from change in the electronic state of square-pyramidal coordinated cobalt.

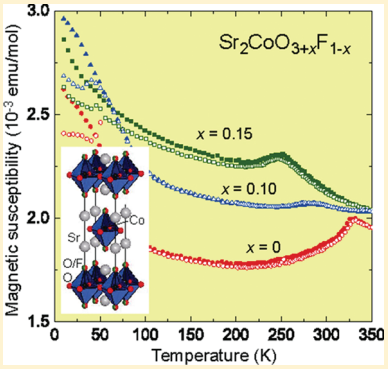

1. INTRODUCTION

Cobalt oxides with the perovskite structure have been drawing much attention because of their attractive physical properties originating from the covalent interactions between the metal center and the oxide anion and the competitions between spin, charge, and orbital degrees of freedom in these materials, for example, high-spin (HS) to low/intermediate-spin (LS/IS) state transition,[1−5] metal−insulator transition, and magneto-resistance phenomenon.[6−9] While these properties are known to be finely controlled by cation substitution,[5,6,8,9] the studies focusing on the effect of anion substitution on the related cobalt oxides have been conducted to a lesser extent. Given that the anion directly affects the crystal field or electronic state of the metal center, the substitution of oxide anion by the anions with different valence, ionic radius, and bonding nature provides good opportunities for inducing the physical properties that cannot be achieved by cation substitution.

In general, it is very difficult to stabilize two kinds of hetero anions in one structure or control their anion compositions because of the large difference of vapor pressures between oxygen and the other anion. Nevertheless, several mixed anion perovskite materials, mainly with layered structures, were successfully obtained to date. For example, Cava et al. synthesized Ruddlesden−Popper (R-P) type layered cobalt oxyhalides, $Sr_{n+1}Co_nO_{2n+1}Cl_n$,[10] where Cl atom occupies preferentially at the terminal apical anion sites, leading to distorted square pyramidal coordination around Co atom (see Figure 1a). Weller et al. have extended to doubly halogenated $Sr_2CoO_2X_2$ (X = Cl, Br) where Co atom is coordinated to four O atoms in a square planar arrangement with X being at the apical sites.[11] On the other hand, Hayward et al. demonstrated

Received: January 17, 2012
Published: April 3, 2012

   dx.doi.org/10.1021/ic300116h | Inorg. Chem. 2012, 51, 4802−4809

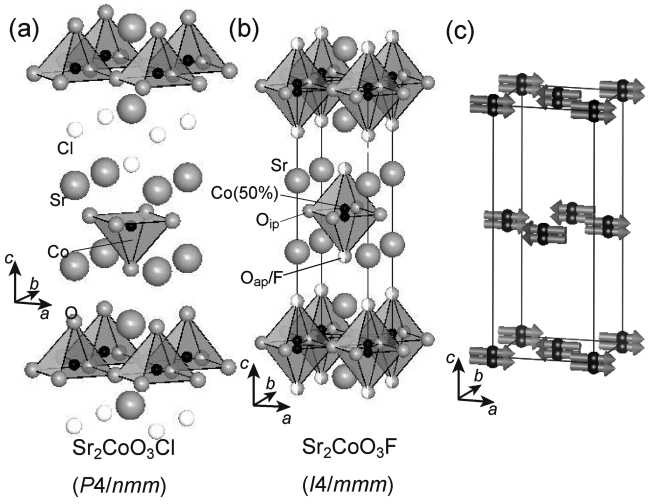

Figure 1. Crystal structures of (a) Sr_2CoO_3Cl with the O/Cl site order and (b) Sr_2CoO_3F with the O/F site disorder. The Co atoms in the latter are randomly displaced along the *c* axis from the center position of the octahedron. Large and small gray, black, and white spheres represent Sr, O, Co, and Cl/F, respectively. (c) Magnetic structure of Sr_2CoO_3F. For clarity, only Co atoms and moments are displayed. The solid line denotes the chemical unit cell in panels *a* and *b* and the magnetic unit cell in panel *c*.

the synthesis of cobalt oxyhydride, $LaSrCoO_3H_{0.7}$[12] and $Sr_3Co_2O_{4.33}H_{0.84}$,[13] using a low-temperature reduction technique. Compared with oxyhalide compounds, H atoms are located within the equatorial anion sites.

One decade ago, Wu carried out the density functional calculations on Sr_2CoO_3Cl and related cobalt oxides with buckled CoO_2 planes.[14] Sr_2CoO_3Cl was shown to be classified as the charge-transfer material.[14,15] The author proposed that injection of (pdσ) holes more than 0.3 in bands consisting of Co 3d(x^2-y^2) and O 2p orbitals or decrease in displacement (D) of Co atoms from the basal plane ($D \leq 0.25$ Å) possibly induces the insulator−metal (I-M) and/or antiferromagnetic-ferromagnetic (AFM-FM) phase transitions. The magnetic and electric ground states of Sr_2CoO_3Cl (D = 0.325 Å at room temperature (RT)) are AFM insulator with T_N = 330 K,[10,16] and the holes per CoO_2 basal square that were calculated on the assumption of ferromagnetic state are only 0.07,[14] insufficient to induce FM metallicity. Wu suggested that replacement of Cl by F with smaller ionic size could lead to AFM-FM and/or I-M transitions, but there were no reports of such substitution study aiming to alter the physical properties of the cobalt oxychloride.

Recently, some of us reported a new class of mixed anion cobalt compound, namely, Sr_2CoO_3F, which was synthesized at 1700 C° under a high pressure of 6 GPa.[17] This compound is the first example of layered cobalt oxyfluoride. As shown in Figure 1b, Sr_2CoO_3F is isostructural to Sr_2CoO_3Cl and has square-pyramidal coordinated Co atoms. The O/F atoms, however, are disordered at the apical sites, which is in contrast to the O/Cl site order in the oxychloride. We are also aware of unusual coordination environment in Sr_2CoO_3F by comparing with other oxyfluoride analogues. For example, Sr_2FeO_3F takes square pyramidal coordination around Fe, but the O/F anions at the apical sites are ordered.[18] On the other hand, O/F anion disorder was observed in K_2NbO_3F[19] and Ba_2ScO_3F[20] with d^0 electronic configuration, but the metal center takes octahedral coordination. Therefore, coexistence of square pyramidal coordination around the metal center and O/F anion disorder, which is probably caused by denser environment or entropic effects, is realized in the cobalt oxyfluoride for the first time.[21] On the basis of the preliminary structure analysis, the D value of Sr_2CoO_3F is ∼0.20 Å, suggesting that it is a ferromagnetic metal. In contrast to Wu's conjecture, the magnetic susceptibility measurements showed a broad peak originating from two-dimensional (2D) antiferromagnetic correlation at around 320 K, not ferromagnetic behavior. To clarify the relationship among the structural, magnetic, and electrical properties in Sr_2CoO_3F, further investigation is necessary.

In this paper, we report the detailed crystal and magnetic structures, magnetic and transport properties of Sr_2CoO_3F investigated by synchrotron powder X-ray and neutron powder diffraction studies, magnetic susceptibility, and electrical resistivity measurements. We also studied the influence of anion substitution and mechanical pressure on the physical properties.

2. EXPERIMENTAL SECTION

High-pressure synthesis is a useful reaction method for preparing mixed anion systems and controlling the anion compositions according to the nominal compositions because the starting materials are reacted in a closed and dense environment. First, we optimized the reaction condition (time and temperature) of Sr_2CoO_3F to reduce the amount of the uncharacterized impurity phases detected in the previous report,[17] then the synthesis of a series of $Sr_2CoO_{3+x}F_{1-x}$ ($x \geq 0.10$) was conducted on the basis of the reaction condition for x = 0. A pressure of 6 GPa was used as reported previously.[17] A stoichiometric mixture of SrO_2, Co, and SrF_2 was ground thoroughly in an Ar-filled glovebox, put into a Pt capsule, and then heated at 1700−2000 °C for 0.5−1.5 h in a belt-type high-pressure apparatus. Among the reaction conditions we tried, we found that heating at 1900 °C for 0.5 h gave the best sample quality.

Synchrotron X-ray diffraction (SXRD) data of all the x compositions were collected using the Debye−Scherrer camera installed on NIMS beamline at SPring-8 with λ = 0.65298 Å.[22] The samples were put in a glass capillary of 0.1 mm in radius, and their data were recorded in 0.003° increments in a 2θ range of 2 to 50°. Neutron powder diffraction (NPD) data were also collected on the high-resolution powder diffractometer (HRPD) installed at HANARO reactor at the Korean Atomic Energy Research Institute (KAERI) in Korea. A sample of 1.6 g was placed in a vanadium cylinder. The data were recorded in 0.05° increments in a 2θ range of 10 to 130°. The wavelength employed was 1.834 Å. The SXRD and NPD data were analyzed by the Rietveld method with the program RIETAN-FP[23] and FullProf,[24] respectively.

Magnetic susceptibility measurements were conducted in an applied magnetic field of H = 1 kOe in the temperature of T = 10−350 K, using a superconducting quantum interface device (SQUID) magnetometer (Quantum Design, MPMS). Electrical resistivity measurements at ambient pressure were performed on a hand-pressed powder sample in the range of 10 ≤ T ≤ 300 K, using a dc four-terminal method in H = 0 and 50 kOe. The pressure dependence of electrical resistivity for x = 0 was also measured by a two-terminal method in the range from P = 0 to 8 GPa, using a cubic anvil-type high-pressure apparatus installed at Tokyo Institute of Technology. A disk-shaped sample (3.5 diameter and 1.4 mm thickness) was used without crushing the as-synthesized sample.

3. RESULTS

3.1. Synthesis and Structure. Figure 2 shows a comparison of SXRD patterns for $Sr_2CoO_{3+x}F_{1-x}$ (x = 0, 0.10, 0.15, 0.20) measured at room temperature. The SXRD data of x = 0 phase prepared at 1900 °C showed significant reduction of impurity phases compared with the sample

dx.doi.org/10.1021/ic300116h | Inorg. Chem. 2012, 51, 4802−4809

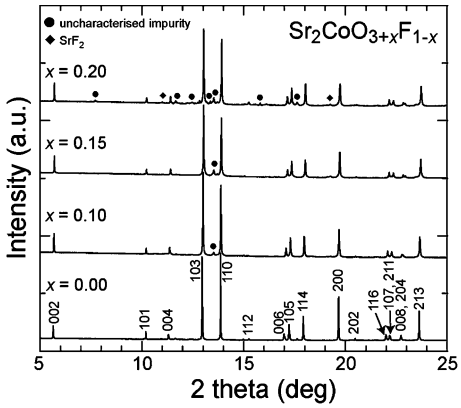

Figure 2. Synchrotron powder X-ray diffraction patterns collected at room temperature from $Sr_2CoO_{3+x}F_{1-x}$ (x = 0, 0.10, 0.15, and 0.20).

prepared at 1700 °C,[17] and could be readily indexed with the simple body centered tetragonal cell in the space group of $I4/mmm$, which is consistent with the previous report.[17] The x = 0.10, 0.15, and 0.20 phases were also obtained as the main phase, but several tiny peaks were additionally detected. If symmetry lowering associated with O/F site ordering as in Sr_2CoO_3Cl ($P4/nmm$) occurs, superlattice reflections are expected to appear in the diffraction patterns. However, there were no extra peaks that could be assigned as $P4/nmm$. Thus, the additional peaks observed should come from impurity phases including SrF_2, although some of them could not be identified. The lattice parameters and volume calculated by the least-squares method for x = 0 are a = 3.8246(2) Å, c = 13.2687(8) Å, and V = 194.09(2) Å^3, which agree well with those reported previously.[17] As shown in Figure 3, the cell parameters monotonically decreased with increasing $x \leq 0.15$ and approached those of Sr_2CoO_4 (x = 1.0; a = 3.796 Å, c = 12.487 Å, V = 179.97 Å^3).[25] This indicates that the O/F

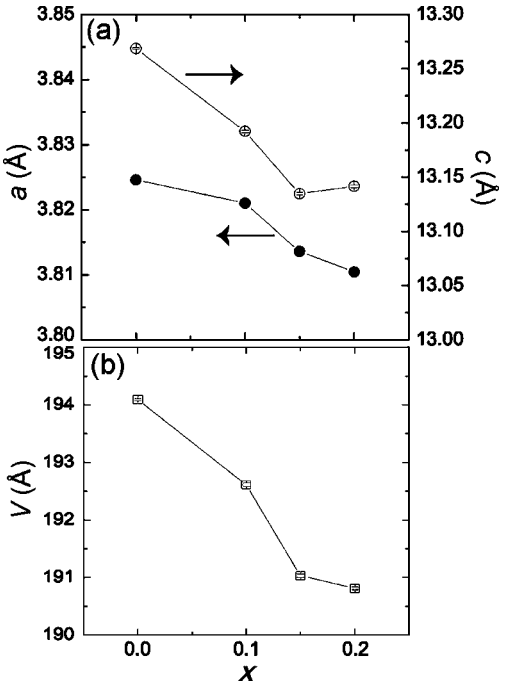

Figure 3. Evolution with x of (a) the lattice constants and (b) volume of $Sr_2CoO_{3+x}F_{1-x}$ (x = 0, 0.10, 0.15, and 0.20).

composition is close to the nominal composition in the x range of 0−0.15. At x = 0.20, however, the cell parameters remained almost unchanged in comparison with those of x = 0.15, suggesting unsuccessful substitution of O for F beyond x = 0.15. Indeed, the number of impurity peaks distinctly increased at x = 0.20. We tried synthesizing $x \geq 0.20$ phases by controlling the reaction temperature and time, but could not achieve it because of two-phase separation or impurity formation.

3.2. Neutron Powder Diffraction. We conducted the neutron powder diffraction experiments to analyze the crystal and magnetic structures of Sr_2CoO_3F (x = 0) in detail. As shown in Figure 4a, major peaks of the NPD patterns collected

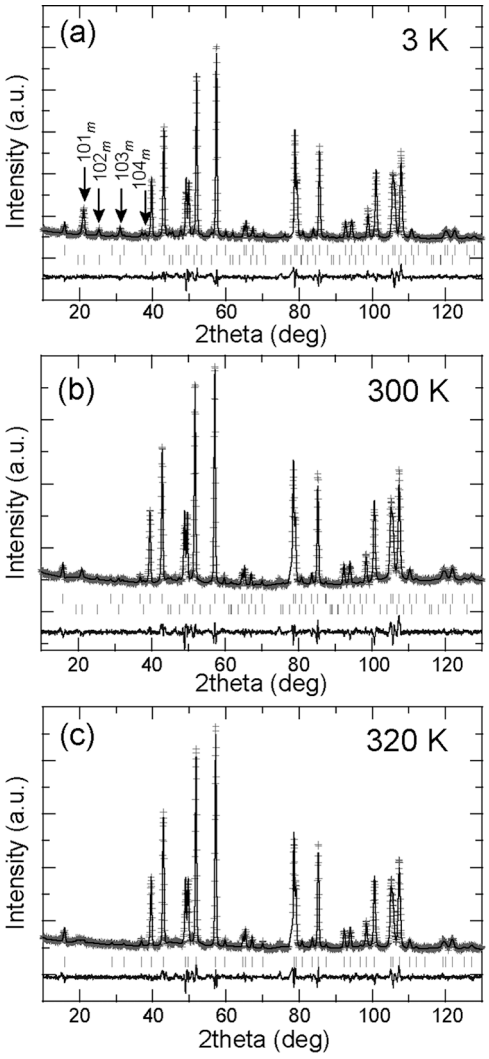

Figure 4. Observed (crosses), calculated (upper solid line), and difference (bottom solid line) plots from the Rietveld structure refinement against the neutron powder diffraction data collected from Sr_2CoO_3F at 3, 300 ($<T_N$), and 320 K ($>T_N$). The nuclear and magnetic Bragg reflections are indicated by the bottom and upper vertical lines, respectively.

at 3 K could be also indexed with the simple body centered tetragonal cell as in the SXRD data. However, several additional peaks which could not be accounted by $I4/mmm$ were discernible, especially in a low angle region. These peaks are likely to be attributed to magnetic origin rather than some impurity phases or lowering crystal symmetry, because the

dx.doi.org/10.1021/ic300116h | Inorg. Chem. 2012, 51, 4802−4809

Table 1. Crystallographic Data of Sr_2CoO_3F at Various Temperatures ($3 \leq T \leq 320$ K) Determined by the Neutron Powder Analysis

	T (K)						
	3	100	200	250	300	310	320
a	3.81933(6)	3.82090(6)	3.82520(6)	3.82800(6)	3.83020(6)	3.83148(7)	3.83172(5)
c	13.2356(4)	13.2400(4)	13.2546(5)	13.2618(5)	13.2696(4)	13.2702(4)	13.2735(4)
V	193.072(8)	193.296(8)	193.944(9)	194.333(9)	194.671(8)	194810(9)	194.884(8)
Sr z	0.36182(11)	0.36189(12)	0.36192(12)	0.36209(12)	0.36235(12)	0.36214(13)	0.36235(12)
Sr B_{iso}/Å^2	0.70(3)	0.62(3)	0.62(3)	0.69(3)	0.68(3)	0.85(3)	1.06(3)
Co z	0.0208(7)	0.0204(8)	0.0203(9)	0.0204(8)	0.0190(10)	0.0196(11)	0.0195(9)
Co B_{iso}/Å^2	0.2(2)	0.3(2)	0.4(2)	0.2(2)	0.9(2)	0.6(2)	0.9(2)
O_{ip} B_{iso}/Å^2	1.18(4)	1.20(4)	1.19(4)	1.12(4)	1.21(4)	1.26(5)	1.38(4)
O_{ap}/F z	0.17416(16)	0.17409(17)	0.17444(18)	0.17434(18)	0.17414(17)	0.17407(18)	0.17428(17)
O_{ap}/F B_{iso}/Å^2	1.02(3)	1.07(4)	1.17(4)	1.21(4)	1.18(4)	1.34(4)	1.58(4)
$\|\mu\|/\mu_B$	3.18(5)	2.96(5)	2.54(5)	1.97(5)	1.48(5)	1.20(5)	0
R_{wp}/%	5.82	5.92	5.89	5.71	5.38	5.78	5.04
R_p/%	4.39	4.41	4.43	4.39	4.16	4.48	3.88
S	2.11	2.16	2.15	2.06	1.86	2.11	1.83

Table 2. Select Bond Lengths and Angles for Sr_2CoO_3F

	T (K)						
	3	100	200	250	300	310	320
				Bond Length/Å			
Sr−O_{ap}/F×2	2.484(3)	2.486(3)	2.485(3)	2.490(3)	2.497(3)	2.496(3)	2.496(3)
	2.7423(4)	2.7435(5)	2.7474(5)	2.7496(5)	2.7513(5)	2.7515(5)	2.7527(5)
Sr−O_{ip}	2.6442(10)	2.6445(11)	2.6472(11)	2.6473(11)	2.6465(11)	2.6489(12)	2.6474(11)
Co−O_{ap}/F×2	2.030(10)	2.035(11)	2.043(12)	2.042(11)	2.059(13)	2.050(15)	2.050(12)
	2.580(10)	2.575(11)	2.581(12)	2.583(11)	2.563(13)	2.570(15)	2.572(12)
Co−O_{ip}	1.9294(13)	1.9294(15)	1.931(2)	1.9330(15)	1.932(2)	1933(2)	1.933(2)
				Bond Angle/deg			
O_{ip}−Co−O_{ip}	163.6(3)	163.9(4)	164.0(4)	163.9(4)	165.0(4)	164.5(4)	164.6(6)

magnetic susceptibility measurements, which will be discussed later, revealed the onset of antiferromagnetic order at T_N = 323(2) K. The most intense magnetic peaks were identified as the 1 0 m (m = 1, 2, 3, 4) reflections on the basis of the magnetic cell $a_m = b_m = \sqrt{2}a_n$, $c_m = c_n$ where a_n and c_n are the nuclear unit cell parameters. Similar behavior was often seen in R-P type layered systems, for example, Sr_2CoO_3Cl,[16] $Sr_2CoO_2X_2$,[26] and Rb_2FeF_4[27] with a propagation vector k = (1/2 1/2 0).

Initially, the nuclear structure was determined by Rietveld refinement of the 3 K NPD data, using the atomic coordinates ($I4/mmm$) reported previously as a starting model. All the atomic coordinates and displacement parameters (B_{iso}) were allowed to vary during the refinement while the site occupancies (g) of all the atoms were fixed at the initial stage. We confirmed that the refinement readily converged well. Then, various collinear spin models consistent with the crystallographic symmetry were examined while all the crystallographic parameters including g were allowed to refine. The occupancies of O_{ip} and O_{ap}/F at the equatorial and apical sites, respectively, did not deviate from the full fraction within experimental error, thus all of them were fixed at unity. The best fit was obtained by a simple G-type antiferromagnetic model with magnetic moments being aligned along the x direction, as shown in Figure 1c. The finally obtained crystallographic data including atomic coordinates, and the selected bond lengths and angles, are tabulated in Tables 1 and 2, respectively. Observed, calculated, and difference plots are shown in Figure 4a. The previous structure refinement against the SXRD data gave an extraordinarily large B_{iso} value (= 3.2 Å^2) of O_{ap}/F. However, the B_{iso} parameter refined using the NPD data in this study resulted in a reasonable value, indicating that O_{ap}/F stayed at the 4e special position. The magnitude of the refined magnetic moment is μ = 3.18(5) μ_B per cobalt atom, consistent with the high spin configuration of Co^{3+} (S = 2).[14,28] The reduction in the magnetic moment in comparison with the expected value of 4 μ_B is probably due to covalency effect of the Co−O bonds in the basal plane and along the z axis. The bond-valence-sum (BVS) calculation performed against Co, O_{ip}, O_{ap}, and F gave the values of 2.60, 2.04, 1.36, and 1.05, respectively. The BVS values of O_{ip} and F ions are consistent with those expected from the composition, but the others significantly deviate from the expected values. Similar results were previously reported.[17] These unusual BVS values possibly originate from a strong hybridization between cobalt $3d_{z^2}$ and oxygen $2p_z$ orbitals along the z axis, which results in the reduction of the magnetic moment of cobalt much larger than the Co−O bonds within the buckled CoO_2 plane does.

Figure 5 shows the temperature evolution of the NPD patterns in the range of $12 \leq 2\theta \leq 24°$ including 0 0 2_n and 1 0 1_m Bragg reflections and the magnetic moment estimated from the Rietveld refinement. The 1 0 1_m peak intensity or ordered magnetic moment gradually decreased with increasing temperatures and vanished at 320 K. This is consistent with the results of the magnetic susceptibility measurements. Close inspection of the peak shape centered at around 21° revealed weak diffuse

dx.doi.org/10.1021/ic300116h | Inorg. Chem. 2012, 51, 4802−4809

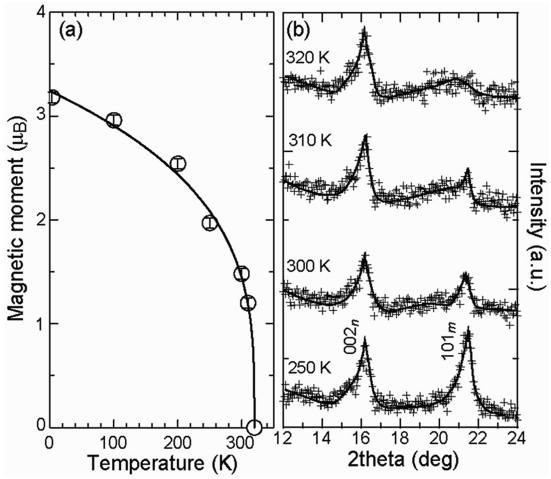

Figure 5. (a) Temperature variation of the magnetic moment of cobalt. The solid line denotes the fit by a power low of $\mu(T)/\mu(0) = C(1 - T/T_N)^{\beta}$ where β is a critical exponent. (b) Temperature variation of the neutron powder diffraction patterns in the range of $12° \leq 2\theta \leq 24°$.

scattering at 320 K, rather than magnetic Bragg reflection. This behavior should be attributed to 2D spin−spin correlations within the CoO_2 planes, which were gradually developed to three-dimensional (3D) long-range magnetic order below 320 K. The diffuse scattering displaying a broad and asymmetric peak persisted even at 300 K but disappeared at 250 K. A layered analogue Sr_2CoO_3Cl was also reported to exhibit similar diffuse scattering with the correlation length ξ of 40 Å just above T_N (= 330 K). The ξ in the present compound could not be estimated accurately because of the poor resolution.[16] The results of the Rietveld refinements using the NPD data collected at 300 and 320 K ($\approx T_N$) are shown in Figure 4. The refined crystallographic data at all the measured temperatures are tabulated in Table 1.

3.3. Synchrotron Powder X-ray Diffraction. The Rietveld fit to the SXRD data collected at room temperature from $Sr_2CoO_{3+x}F_{1-x}$ (x = 0, 0.10 and 0.15) is shown in Supporting Information, Figure S1. The structure refinement using the SXRD data in the x range converged immediately when the same model of x = 0 determined by the NPD refinement was assumed as the starting model. The refined crystallographic data are shown in Table 3, where no noticeable difference was discernible among each of the x values: Co atoms maintain square pyramidal coordination against anions with the apical anions being disordered, although the gradual volume reduction with increasing x was accompanied by the systematic contraction of the bond lengths between Co and the neighboring anions. The BVS values of Co and O_{ap} also remain far from their expected values. Common to all the x, the atomic displacement parameter of O_{ap}/F is relatively large, as in the SXRD refinement reported previously.[17] Such a large value is basically caused by either anion deficiency or site disordering, which contradicts the results of the NPD refinements described above. Thus, the large B_{iso} values for O_{ap}/F may be simply attributed to poor sensitivity to light elements on the SXRD measurements.

3.4. Magnetic Susceptibility and Electrical Resistivity. Figure 6 shows the temperature dependence of the magnetic susceptibilities ($\chi(T) = M/H$) for x = 0, 0.10, and 0.15, measured in an applied magnetic field of H = 1 kOe under zero

Table 3. Crystallographic Data of $Sr_2CoO_{3+x}F_{1-x}$ (x = 0, 0.10, 0.15) at Room Temperature Determined by the Synchrotron Powder X-ray Analysis

x	0	0.10	0.15
a	3.82197(2)	3.82102(1)	3.81339(1)
c	13.26686(3)	13.19116(5)	13.13148(6)
V	193.7949(6)	192.5937(10)	190.9573(10)
Sr z	0.36190(3)	0.36239(3)	0.36222(4)
Sr B_{iso}/Å^2	0.743(8)	0.776(17)	0.701(9)
Co z	0.01885(11)	0.01899(13)	0.01865(14)
Co B_{iso}/Å^2	0.11(2)	0.30(3)	0.15(3)
O_{ip} B_{iso}/Å^2	0.18(5)	1.22(7)	0.48(7)
O_{ap}/F z	0.17107(16)	0.17082(18)	0.1709(2)
O_{ap}/F B_{iso}/Å^2	2.72(5)	2.47(5)	2.68(6)
R_{wp}/%	1.33	1.24	1.38
R_p/%	0.85	0.85	0.85
R_I/%	5.63	4.73	5.17
BVS Sr	1.91	1.96	2.00
BVS Co	2.64	2.67	2.71
BVS O_{ap}	2.04	2.07	2.10
BVS O_{ip}	1.34	1.36	1.39
BVS F	1.04	1.05	1.07

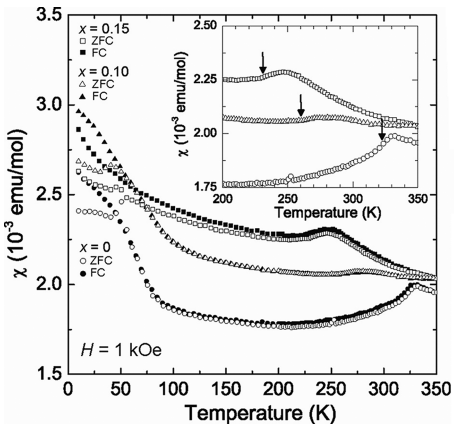

Figure 6. Magnetic susceptibility $\chi(T)$ of $Sr_2CoO_{3+x}F_{1-x}$ as a function of temperature, measured in an applied magnetic field of H = 1 kOe. The inset shows the χ data measured under zero field cooled condition in the range of $200 \leq T \leq 350$ K. The arrows denotes the temperature where $\chi(T)/dT$ took a maximum value associated with the onset of magnetic long-range order.

field cooling (ZFC) and field cooling (FC) conditions. $\chi(T)$ of x = 0 exhibited a clear drop at 332 K indicative of the antiferromagnetic correlation. In light of the 2D magnetism in this compound, the temperature derivative of $\chi(T)$ is more appropriate for determining the Néel temperature. Thus, the T_N estimated from the temperature at which $\chi(T)/dT$ took a maximum value is 323(2) K. This is consistent with the results of the neutron diffraction experiments. Ten and 15%-O substitution lowered T_N to 260 and 230 K, respectively (see the inset of Figure 6). We attempted to fit the magnetic susceptibility data to the Curie−Weiss law, but it was not successful because of the absence of the linear part appropriate for the fit above T_N. The divergence between ZFC and FC data below T_N should be attributed to some impurities. In light of the ferromagnetic behavior observed in Sr_2CoO_4,[25] ferromagnetic interactions between Co^{4+}-O^{2-}-Co^{4+} in the CoO_2,[29] which were introduced by F-to-O substitution, can contribute to the gradual suppression of T_N.

dx.doi.org/10.1021/ic300116h | Inorg. Chem. 2012, 51, 4802−4809

Figure 7 shows the temperature dependence of the electrical resistivity $R(T)$ at ambient pressure and zero magnetic field for

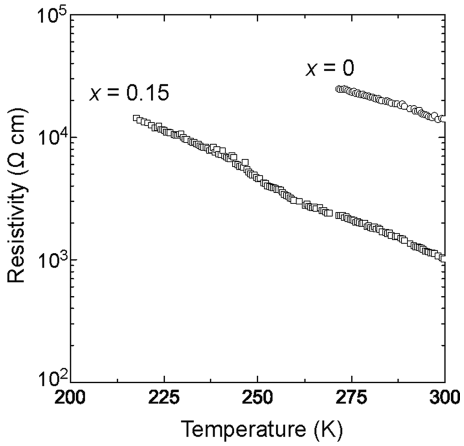

Figure 7. Temperature dependence of the electrical resistivity for $x = 0$ (open circles) and 0.15 (open squares), measured in zero magnetic field.

$x = 0$ and 0.15. The D values for $x = 0$ and 0.15 at 300 K are 0.25 and 0.244 Å, respectively, nearly close to the critical value, where AFM-FM and/or I-M transition could be expected to occur. However, we found that both x's exhibited insulating behavior down to the temperature where $R(T)$ became immeasurably large, although the resistivity of $x = 0.15$ was smaller by one degree of magnitude than that of $x = 0$. We also examined the magnetic field dependence of $R(T)$ in an applied magnetic field of $H = 50$ kOe, but could not observe a magnetoresistance effect. This is in contrast to the electrical resistivity of half metallic Sr_2CoO_4 showing the negative magnetoresistance of ~4% at T_C.[25]

Pressure can effectively alter the structural, magnetic, and transport properties of transition metal compounds through changes in the metal−ligand bonding states, leading to I-M transition or spin state transition.[30−33] Sr_2CoO_3Cl is a charge-transfer material with the d orbital splitting into b_{2g} (d_{xy}), doubly degenerate e_g (d_{xz}, d_{yx}), a_{1g} (d_{z^2}) and b_{1g} ($d_{x^2-y^2}$).[14] Thus, we can expect under pressure an I-M transition or a spin state transition caused by the closure of the charge-transfer gap or further splitting of the crystal field. Figure 8 shows the

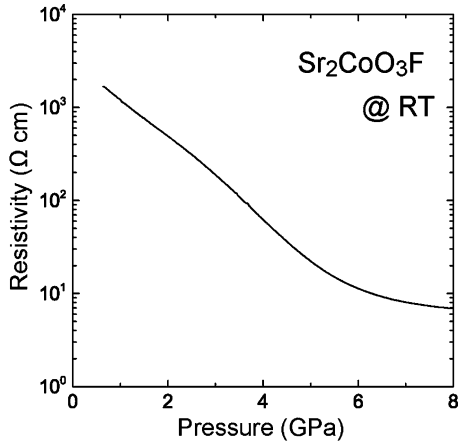

Figure 8. Pressure dependence of the electrical resistivity at room temperature for Sr_2CoO_3F.

pressure dependence of $R(P)$ for Sr_2CoO_3F ($x = 0$). Interestingly, $R(P)$ decreased by more than two degrees of magnitude in the range of $0.7 < P \leq 8$ GPa, implying the onset of the metallic state. Similar pressure induced insulator−metal phase transition was seen in square pyramidal coordinated cobalt oxides such as $BiCoO_3$[2] and $TbBaCo_2O_{5.5}$.[34] However, this type of phase transition has not been observed in any mixed anion cobalt perovskites. The gradual decrease of resistivity suggests that the I-M phase transition is a second order one.

4. DISCUSSION

We have shown that Sr_2CoO_3F undergoes an antiferromagnetic long-range ordering in the high-spin state ($S = 2$) of Co^{3+} at 323 K. In particular, the neutron diffraction study revealed that the magnetic behaviors of Sr_2CoO_3F are very similar to those of the isostructural compound Sr_2CoO_3Cl ($T_N = 330$ K) as follows: (i) T_N's for the two compounds are close to each other. Given the layered structure separating the CoO_2 planes, the superexchange pathways through $Co-O_{ip}-Co$ in the CoO_2 planes mostly dictate their magnetic nature in comparison with those bridging between the nearest neighbor CoO_2 planes. (ii) The magnetic structure or spin arrangement, which is described as a simple G-type antiferromagnetic order with $k = (1/2\ 1/2\ 0)$, is the same between Sr_2CoO_3X (X = F, Cl). Strictly speaking, Sr_2CoO_3Cl has alternate stacking of CoO_2 planes with shorter and longer Co−Co distances along the c axis, because of the O/Cl order at the apical sites. (see Figure 1a). However, such anion order/disorder does not appear to influence the spin arrangement, which is consistent with weak superexchange interactions between the CoO_2 planes. (iii) The temperature evolution of magnetic ordered state for Sr_2CoO_3F, traces that for Sr_2CoO_3Cl. As shown in Figure 5a, we fitted the sublattice magnetization data in the temperature range of 3 to 320 K, using a power law of $\mu(T)/\mu(0) = C(1 - T/T_N)^{\beta}$, yielding $C = 1.01(2)$, $T_N = 320(6)$ K, and critical exponent $\beta = 0.29(4)$. The value of μ (3 K) was taken as $\mu(0)$. The obtained β value is almost the same as that estimated from the oxychloride ($\beta = 0.28(3)$) and suggests the magnetic phase transition in these oxyhalide compounds is 3D in nature rather than of 2D Ising character ($\beta = 0.125$), which was observed in isostructural systems such as K_2NiF_4[27] and Rb_2CoF_4.[35] The 3D character observed may be associated with the cobalt site at which the internal magnetic field from the nearest neighbor CoO_2 layers cannot be canceled out to zero in total, because of O/(F, Cl) occupation at the apical sites. Such a relationship between magnetic interactions and structural feature is likely to deteriorate the 2D magnetic nature more or less.

Figure 9 shows the temperature dependences of the lattice parameters and cell volume for Sr_2CoO_3F over the range of $3 \leq T \leq 320$ K, obtained from the NPD experiments. The corresponding evolutions of bond lengths and angles around the Co atoms are shown in Figure 10. The cell parameters including a, c, and V systematically decreased with decreasing temperatures. On the other hand, large variation in the coordination environment around Co was observed between 250 and 300 K. As shown in Figure 10a, the short (long) $Co-O_{ap}/F$ bond decreased (increased) with decreasing temperatures. By analogy with the coordination environment in Sr_2CoO_3Cl (see Figure 1a), the short and long $Co-O_{ap}/F$ bonds should be associated with $Co-O_{ap}$ and Co−F bonds, respectively, although it is not possible to strictly distinguish these two bonds because the refined structure is an averaged

dx.doi.org/10.1021/ic300116h | Inorg. Chem. 2012, 51, 4802−4809

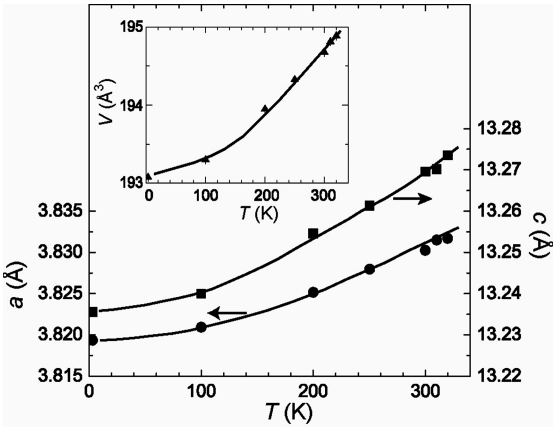

Figure 9. Temperature evolution of the lattice constants and volume for Sr_2CoO_3F. Solid circles, squares, and triangles represent the *a*, *c*, and *V*, respectively.

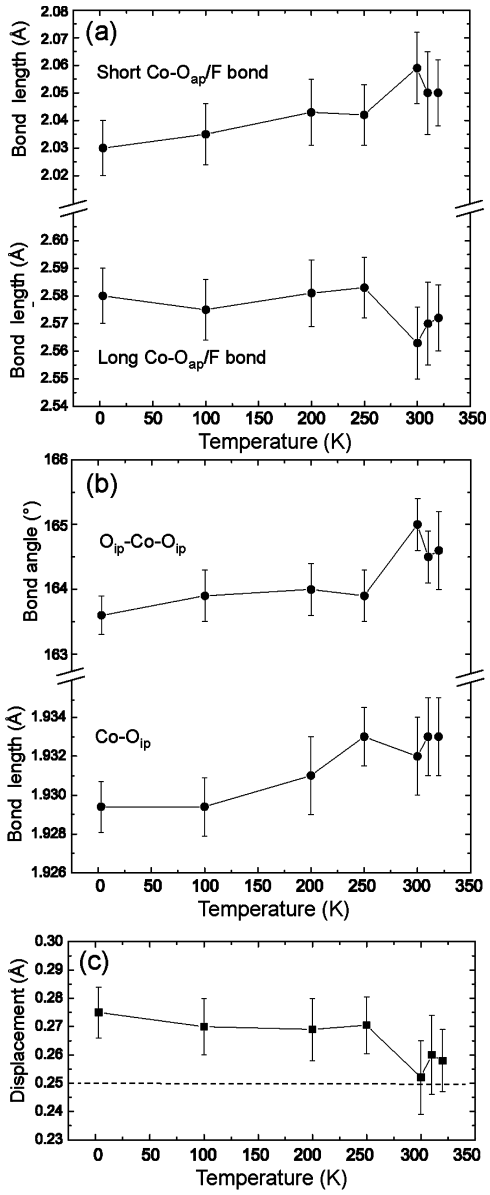

Figure 10. Temperature dependence of the cobalt environment in Sr_2CoO_3F. The dashed line in panel *c* coincides with D = 0.25 Å.

one. Indeed, the Co−O_{ap} (Co−Cl) bond in Sr_2CoO_3Cl at 3 K is contracted (elongated) in comparison with the room temperature data. Given the strong orbital hybridization between Co and O_{ap} atoms, these results are reasonable.

Finally we discuss the relationship among the structural, magnetic, and transport properties in $Sr_2CoO_{3+x}F_{1-x}$. The temperature dependence of D for x = 0 is shown in Figure 10c. The D values at 300 K and above are located at 0.25−0.26 Å. On further cooling, the D value increased to ∼0.275 Å with temperature and the O_{ip}−Co−O_{ip} basal bond angle shown in Figure 10b became further buckled. According to the conjecture by Wu, the AFM-FM and/or I-M transition possibly occur at D = 0.25 Å, namely, at ∼300 K. However, no noticeable anomaly except an AFM transition at 323 K was observed. 15%-O substitution for F at the apical sites, namely, x = 0.15, resulted in the reduction of the D value to 0.244 Å, smaller than the critical value. Nevertheless, the AFM/I state still persisted as shown above. These experimental findings suggest that p-d exchange associated with pdσ hole delocalization is too weak to induce ferromagnetic metallicity. On the other hand, Sr_2CoO_3F exhibited the onset of the metallic state at room temperature by applying pressure, which is associated with I-M transition. Such a pressure-induced phase transition in cobalt compounds generally involves changes in the coordination environment and spin state of the cobalt cation. For example, a $PbTiO_3$-type perovskite $BiCoO_3$ (5-fold coordination) exhibits the abrupt reduction of resistivity at 2−3 GPa, followed by the structural phase transition to $GdFeO_3$-type structure (6-fold coordination) and the HS-LS state phase transition. The phase transition is first order. The gradual decrease of resistivity in Sr_2CoO_3F, however, suggests a second order phase transition. Although we do not have any information on the pressure dependence of the structure and spin state at this stage, gradual suppression of buckling within the CoO_2 basal plane and/or continuous depopulation of the HS state with pressure likely resulted in the observed resistivity reduction. Understanding the mechanism of resistivity reduction under pressure is an interesting future work.

5. CONCLUSION

We investigated the structural, magnetic, and transport properties of $Sr_2CoO_{3+x}F_{1-x}$ by powder X-ray synchrotron and neutron powder diffraction studies, magnetic susceptibility and electrical resistivity measurements. Sr_2CoO_3F adopts a G-type antiferromagnetic ordered structure below T_N = 323 K with the magnetic moment of 3.18 μ_B per cobalt, consistent with the high-spin state of Co^{3+}. The antiferromagnetic and insulating states persist even on 15%-O substitution for F at the apical sites, although T_N and electrical resistivity decrease when increasing the substitution amount. In contrast, applying pressure on Sr_2CoO_3F induces the significant reduction in resistivity, namely, the onset of insulator−metal phase transition. We believe that further investigation in a wider range of pressure should unveil the strong correlation among spin, charge, and orbital degrees of freedom that is hidden at ambient pressure.

■ ASSOCIATED CONTENT

Ⓢ Supporting Information

The results of the structure refinement using the SXRD data collected from x = 0, 0.10, and 0.15. This material is available free of charge via the Internet at http://pubs.acs.org.

dx.doi.org/10.1021/ic300116h | Inorg. Chem. 2012, 51, 4802−4809

AUTHOR INFORMATION

Corresponding Author

*E-mail: Tsujimoto.Yoshihiro@nims.go.jp.

Notes

The authors declare no competing financial interest.

ACKNOWLEDGMENTS

We thank Y. Katsuya, M. Tanaka, and O. Sakata for supporting the SXRD experiments, and M. Miyakawa, K. Fujimaki, and T. Taniguchi for support with the high-pressure synthesis at NIMS. This work was supported by the World Premier International Research Center (WPI) initiative on Materials Nanoarchitechtonics (MANA), a Grant-in-Aid for "Transformative Research-Project on Iron Pnictides (TRIP)" from JSPS and Grants-in-Aid for Research Activity (22850019 and 21540330) from MEXT in Japan. The NPD experiments were performed under the NIMS-RIKEN-JAEA Cooperative Research Program on Quantum Beam Science and Technology. Finally, we acknowledge the kind allocation of beamtime at HRPD, KAERI.

REFERENCES

(1) Saitoh, T.; Mizokawa, T.; Fujimori, A.; Abbate, M.; Takeda, Y.; Takano, M. *Phys. Rev. B* **1997**, *55*, 4257.

(2) Oka, K.; Azuma, M.; Chen, W.; Yusa, H.; Belik, A. A.; Takayama-Muromachi, E.; Mizumaki, M.; Ishimatsu, N.; Hiraoka, N.; Tsujimoto, M.; Tucker, M. G.; Attfield, J. P.; Shimakawa, Y. *J. Am. Chem. Soc.* **2010**, *132*, 9438.

(3) Nakao, H.; Murata, T.; Bizen, D.; Murakami, Y.; Ohoyama, K.; Yamada, K.; Ishiwata, S.; Kobayashi, W.; Terasaki, I. *J. Phys. Soc. Jpn.* **2011**, *80*, 023711.

(4) Vogt, T.; Woodward, P. M.; Karen, P.; Hunter, B. A.; Henning, P.; Moodenbaugh, A. R. *Phys. Rev. Lett.* **2000**, *84*, 2969.

(5) Moritomo, Y.; Higashi, K.; Matsuda, K.; Nakamura, A. *Phys. Rev. B* **1997**, *55*, R14725.

(6) Briceno, G.; Chang, H.; Sun, X.; Schultz, P. G.; Xiang, X.-D. *Science* **1995**, *270*, 273.

(7) Moritomo, Y.; Akimoto, T.; Takeo, M.; Machida, A.; Nishibori, E.; Takata, M.; Sakata, M.; Ohyama, K.; Nakamura, A. *Phys. Rev. B* **2000**, *61*, R13325.

(8) Maignan, A.; Martin, C.; Pelloquin, D.; Nguyen, N.; Raveau, B. *J. Solid State Chem.* **1999**, *142*, 247.

(9) Yoshida, S.; Kobayashi, W.; Nakano, T.; Terasaki, I.; Matsubayashi, K.; Uwatoko, Y.; Grigoraviciute, I.; Karppinen, M.; Yamauchi, H. *J. Phys. Soc. Jpn.* **2009**, *78*, 094711.

(10) Loureiro, S. M.; Felser, C.; Huang, Q.; Cava, R. J. *Chem. Mater.* **2000**, *12*, 3181.

(11) Knee, C. S.; Weller, M. T. *J. Solid State Chem.* **2002**, *168*, 1.

(12) Hayward, M. A.; Cussen, E. J.; Claridge, J. B.; Bieringer, M.; Rosseinsky, M. J.; Kiely, C. J.; Blundell, S. J.; Marshall, I. M.; Pratt, F. L. *Science* **2002**, *295*, 1882.

(13) Helps, R. M.; Rees, N. H.; Hayward, M. A. *Inorg. Chem.* **2010**, *49*, 11062.

(14) Wu, H. *Eur. Phys. J. B* **2002**, *30*, 501.

(15) Zaanen, J.; Sawatzky, G. A.; Allen, J. W. *Phys. Rev. Lett.* **1985**, *55*, 418. Dagotto, E. *Rev. Mod. Phys.* **1994**, *66*, 763. Imada, M.; Fujimori, A.; Tokura, Y. *Rev. Mod. Phys.* **1998**, *70*, 1039.

(16) Knee, C. S.; Price, D. J.; Lees, M. R.; Weller, M. T. *Phys. Rev. B* **2003**, *68*, 174407.

(17) Tsujimoto, Y.; Li, J. J.; Yamaura, K.; Matsushita, Y.; Katsuya, Y.; Tanaka, M.; Shirako, Y.; Akaogi, M.; Takayama-Muromachi, E. *Chem. Commun.* **2011**, *47*, 3263.

(18) Case, G. S.; Hector, A. L.; Levason, W.; Needs, R. L.; Thoma, M. F.; Weller, M. T. *J. Mater. Chem.* **1999**, *9*, 2821.

(19) Galasso, F.; Darby, W. *J. Phys. Chem.* **1962**, *66*, 1318.

(20) Needs, R. L.; Weller, M. T.; Scheler, U.; Harris, R. K. *J. Mater. Chem.* **1996**, *6*, 1219.

(21) Tsujimoto, Y.; Yamaura, K.; Takayama-Muromachi, E. *Appl. Sci.* **2012**, *2*, 206.

(22) Tanaka, M.; Katsuya, Y.; Yamamoto, A. *Rev. Sci. Instrum.* **2008**, *79*, 075106.

(23) Izumi, F.; Momma, K. *Solid State Phenom.* **2007**, *130*, 15. Momma, K.; Izumi, F. *J. Appl. Crystallogr.* **2011**, *44*, 1272.

(24) Rodriguez-Carvajal, J. *Phys. B* **1993**, *192*, 55.

(25) Wang, X. L.; Takayama-Muromachi, E. *Phys. Rev. B* **2005**, *72*, 064401.

(26) Knee, C. S.; Weller, M. T. *Phys. Rev. B* **2004**, *70*, 144406.

(27) Birgeneau, R. J.; Guggenheim, H. J.; Shirane, G. *Phys. Rev. B* **1970**, *1*, 2211.

(28) Hu, Z.; Wu, H.; Haverkort, M. W.; Hsieh, H. H.; Lin, H. -J.; Lorenz, T.; Baier, J.; Reichl, A.; Bonn, I.; Felser, C.; Tanaka, A.; Chen, C. T.; Tjeng, L. H. *Phys. Rev. Lett.* **2004**, *92*, 207402.

(29) Lee, K. -W.; Pickett, W. E. *Phys. Rev. B* **2006**, *73*, 174428. Pandey, S. K. *Phys. Rev. B* **2010**, *81*, 035114.

(30) Vogt, T.; Hriljac, J. A.; Hyatt, N. C.; Woodward, P. *Phys. Rev. B* **2003**, *67*, 140401(R).

(31) Pasternak, M. P.; Taylor, R. D.; Chen, A.; Meade, C.; Falicov, L. M.; Giesekus, A.; Jeanloz, R.; Yu, P. Y. *Phys. Rev. Lett.* **1990**, *65*, 790.

(32) Pasternak, M. P.; Taylor, R. D.; Jeanloz, R.; Li, X.; Nguyen, J. H.; McCammon, C. A. *Phys. Rev. Lett.* **1997**, *79*, 5046.

(33) Kawakami, T.; Tsujimoto, Y.; Kageyama, H.; Chen; Xing-Qiu, F.; C. L.; Tassel, C.; Kitada, A.; Suto, S.; Hirama, K.; Sekiya, Y.; Makino, Y.; Okada, T.; Yagi, T.; Hayashi, N.; Yoshimura, K.; Nasu, S.; Podloucky, R.; Takano, M. *Nat. Chem.* **2009**, *1*, 371.

(34) Chernyshov, D.; Rozenberg, G.; Greenberg, E.; Pomyakushina, E.; Dmitriev, V. *Phys. Rev. Lett.* **2009**, *103*, 125501.

(35) Samuelsen, E. J. *Phys. Rev. Lett.* **1973**, *31*, 936.